Appl. Phys. A 78, 223–230 (2004)
DOI: 10.1007/s00339-003-2306-2

Applied Physics A
Materials Science & Processing

S. BOROWSKI[1]
T. KLÜNER[1,✉]
H.-J. FREUND[1]
I. KLINKMANN[2]
K. AL-SHAMERY[2]
M. PYKAVY[3,*]
V. STAEMMLER[3]

Lateral velocity distributions in laser-induced desorption of CO from $Cr_2O_3(0001)$: experiment and theory

[1] Fritz-Haber-Institut der Max-Planck-Gesellschaft, Faradayweg 4–6, 14195 Berlin, Germany
[2] Carl v. Ossietzky Universität Oldenburg, Fachbereich 9, Postfach 2503, 26111 Oldenburg, Germany
[3] Lehrstuhl für Theoretische Chemie, Ruhr-Universität Bochum, Universitätsstraße 150, 44780 Bochum, Germany

Received: 30 April 2003/accepted: 4 July 2003
Published online: 31 October 2003 •

ABSTRACT Quantum state resolved determination of lateral velocity distributions in laser-induced desorption of CO from a $Cr_2O_3(0001)$ surface is investigated. Experimentally, Doppler profiles are obtained via a $(1+1')$-REMPI detection scheme for various rovibrational states and desorption velocities. The experimental findings are directly compared to theoretical results from high-dimensional stochastic quantum dynamical wave packet calculations based on complete first-principles potential energy surfaces. Reasonable quantitative agreement between experiment and theory concerning the total width as well as the full width at half maximum of the lateral velocity distributions is found. Depending on the rotational state a single-peaked or a double-peaked shape of the Doppler profiles is predicted theoretically. In order to support our theoretical predictions we suggest refined experimental investigations of the state-resolved Doppler profiles with an enhanced signal to noise ratio and further theoretical studies concerning the nature of the electronically excited intermediate.

PACS 79.20.La

1 Introduction

Solid surfaces can be used as instruments to orient and modify molecules at distances close to molecular bond lengths while light may serve as a tool to start reactions between adjacent molecules.

One of the advantages in using light to start a chemical reaction is its potential for a selective reaction control. As electronically excited states particularly on metals have lifetimes of only a few femtoseconds (fs) before being quenched, the direct application of 'pump and control' techniques as in gas-phase reactions is scarcely possible. However, by choosing the appropriate substrate one may be able not only to alter catalytic activity but also to control the excited-state lifetime intrinsically.

✉ Fax: +49-30/8413-4101, E-mail: kluener@fhi-berlin.mpg.de
*_Present address:_ Institut für Chemie, Sekretariat C3, Fakultät II, Technische Universität Berlin, Straße des 17. Juni 135, 10623 Berlin, Germany

In order to use the full potential of such an approach a detailed understanding of the underlying elementary processes of electronic and nuclear motion and the related time scales is crucial [1–6]. As will be seen below even for simple reactions the processes can be rather complex. Thus, the investigations in fundamental research concentrate mainly on the most simple chemical reaction, the cleavage of the molecule–surface bond followed by desorption of the molecule.

Some attempts have been made to detect desorbing particles with the use of imaging techniques. A common method is the ESDIAD (electron stimulated desorption ion angular distribution) setup that utilizes an imaging plane in front of the crystal surface to detect the desorbing molecules at nearly the same distance in different angular directions [7, 8]. The detection plane consists of a multichannel plate (MCP)-phosphor screen assembly. The use of resonant enhanced multiphoton ionization (REMPI) enables quantum state resolved detection of neutral molecules. The setup can be run in two detection modes:

1.) Integral mode:
In integral mode the delay between desorption and detection is varied. The intensity is recorded for each delay time to obtain an angular averaged desorption velocity distribution by recording all ions arriving at the detector.

2.) Two-dimensional mode:
Detection of the angular distribution for a single desorption velocity is achieved by ionizing the molecules at a fixed time delay between desorption and detection using for example REMPI to obtain quantum state resolved recording of the two-dimensional image in front of the surface. Only molecules with a single desorption velocity can be detected. In principle, time-dependent recording with concomitant spatial resolution allows for the simultaneous acquisition of velocity distributions for single desorption angles; this however necessitates an elaborate data-collection system.

In a second type of setup the imaging plane of the detector is positioned perpendicular to the surface plane [9]. To obtain an image providing information on both angular and desorption velocity distributions the detection laser beam is spread out forming a broad sheet in the detection plane. All

molecules in this sheet are then ionized forming an intensity distribution when using REMPI. The digitized images can be transformed to give desorption velocity and angular distributions from a single set of data.

Both methods mentioned are limited to ionization techniques. Furthermore, both detection schemes could only be used for molecules desorbing with large desorption cross sections and exhibiting a high efficiency with respect to the ionization techniques used. A reasonable signal to noise ratio can only be obtained after averaging over hundreds of laser shots in view of the few molecules locally detected at a certain MCP segment.

Therefore, we introduce measurements of Doppler-limited spectra widely used in gas-phase photochemistry [10, 11] to the investigation of a DIET (desorption induced by electronic transition) process. As a model system we present data on CO desorbing from a $Cr_2O_3(0001)$ oxide film epitaxially grown on a Cr(110) surface.

In order to gain microscopic insight into the physics of laser-induced desorption we performed theoretical investigations which can be directly compared to experimental results. Most simulations of DIET phenomena are based on two-state scenarios [12]. A laser pulse induces a vertical transition of a nuclear wave packet from the electronic ground state to an electronically excited state. Since the topology of the potential energy surfaces (PESs) is different for the two states involved the wave packet evolves in time according to the potential energy gradients of the excited-state PES. In general, this time evolution is associated with a gain of kinetic energy. The lifetime of the electronically excited state is in the order of 10–30 fs for molecules desorbing from insulator surfaces [13, 14]. After spending this time on the excited-state PES the nuclear wave packet is transferred back to the ground-state PES and is propagated in time until the desorption event is complete. Traditionally, DIET processes are interpreted in terms of the MGR (Menzel–Gomer–Redhaed) [15] and Antoniewicz [16] scenarios, respectively. Both models imply the change of distance of the adsorbed molecule from the surface after laser irradiation to be the driving force enabling desorption after relaxation to the electronic ground state. In the MGR model the electronically excited state is assumed to be purely repulsive with respect to the desorption coordinate. Depending on the lifetime of the excited state the gain of kinetic energy might be sufficient to overcome the potential well of the ground state. In the Antoniewicz scenario the molecule is accelerated towards the surface after excitation and desorption takes place in the electronic ground state after backscattering from the surface.

In general, these two scenarios are treated as one-dimensional models in which only the molecule–surface distance is considered as reaction coordinate. While qualitative physical insight might be gained by applying these simplified approaches a detailed investigation poses a challenge to theory. In particular, two major difficulties occur in the quantitative simulation of DIET processes:

1.) Up to now, only empirical studies have been possible since no potential surfaces – especially for the excited electronic states involved in the desorption process – have been available. Besides a three-dimensional calculation of potential energy surfaces for the system investigated in the present study [14] the only exception is a two-dimensional PES calculated by Klüner et al. [13] for the system NO/NiO(100).

2.) Furthermore, almost all simulations of the dynamics of nuclear motion were restricted to a few degrees of freedom. In most studies one- or two-dimensional investigations are reported [12]. Often, the internal molecular vibration was investigated as the second degree of freedom [17]. A two-dimensional approach was crucial to understand isotope effects in photon- or electron-induced desorption of ammonia from metal surfaces [18]. However, a quantitative simulation of the laser-induced desorption process requires the inclusion of all relevant degrees of freedom.

The ultimate goal of the present study is to encounter both challenges: results of high-dimensional wave-packet calculations utilizing ab initio potential energy surfaces will be presented. For the first time, we report four-dimensional stochastic wave packet calculations on ab initio potential energy surfaces for the electronic ground state as well as for the electronically excited intermediate. As a prerequisite for this study not only four-dimensional ab initio potential energy surfaces had to be calculated [19] but also an efficient implementation of our high-dimensional wave packet code on massively parallel supercomputers had to be realized [20]. A direct comparison with experimentally obtained Doppler profiles is performed, and perspectives for future experimental and theoretical studies will be provided.

2 Experimental setup and details of calculation

2.1 *Experimental setup*

The experiments are carried out in a UHV chamber equipped with LEED (low-energy electron diffraction), XPS (X-ray photoelectron spectroscopy), a quadrupole mass spectrometer for residual gas analysis and TDS (thermal desorption spectroscopy). Details of the experimental setup are given elsewhere [9]. A Cr(110) crystal is spot welded to a sample holder attached to a liquid-nitrogen reservoir. The single crystal is cleaned prior to oxidation via neon-ion bombardment and annealing. The film of $Cr_2O_3(0001)$ is epitaxially grown on the cleaned single crystal by oxidizing the crystal in an atmosphere of 10^{-6} Torr of oxygen at 500 K followed by subsequent annealing of the film to 1000 K [21]. The crystal is dosed with CO at 100 K via a background pressure of 2×10^{-7} Torr during the experiments to keep a steady-state coverage. For illustration, Fig. 1 shows a structure model of the CO molecules adsorbed in flat bonding geometry on the Cr-terminated $Cr_2O_3(0001)$ surface [22].

The experiments are of pump–probe type. The desorption process is induced by impinging pulses of a broad-band excimer laser (Lambda Physik EMG 200) at 6.4 eV (pulse length of 15 ns, fluence of maximally 1 mJ cm^{-2}) normal to the surface. After a well-defined time delay the desorbing CO molecules are detected using a laser beam running parallel to the surface at a distance of 29 mm. Variation of time delays between desorption and detection allows us to record desorption

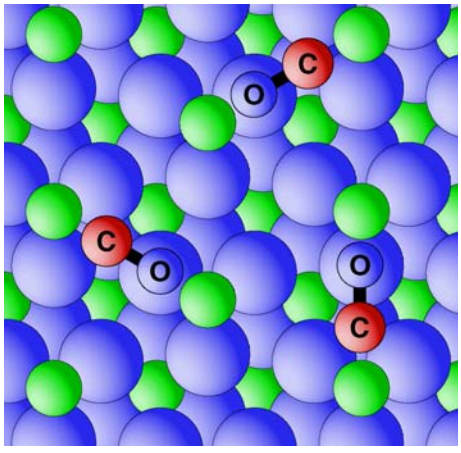

FIGURE 1 Structure model for CO molecules adsorbed on a Cr_2O_3(0001) surface [22]

velocity distributions of single rovibrational states. The detection laser system consists of an excimer laser (XeCl, Lambda Physik LPX 205 I cc) pumped tunable dye laser (Lambda Physik LPD 3002). For Doppler profile measurements it is necessary to use an intracavity etalon to enhance the initial detection laser resolution of 0.2 cm^{-1} to 0.04 cm^{-1}. The detection laser light is linearly polarized and has a triangular beam shape of 2–3 mm in diameter directly at the exit of the laser. A Glan laser prism (Melles–Griot) is used for optimizing the degree of polarization.

A $(1+1')$-REMPI scheme via the $B^1\Sigma^+$ electronic state of CO is employed to detect the desorbing CO molecules' states selectively as described by Rottke and Zacharias [23]. For this purpose fundamental laser light generated at $\lambda =$ 344.0–345.5 nm (6–10 mJ/pulse, using p-terphenyl dissolved in dioxane as dye) is focused (Suprasil B lens, $f =$ 75 mm) into a cell filled with 75 Torr xenon. Via a non-linear process VUV laser light is generated at $\lambda_0 = 114.6$–115.2 nm. By utilizing an ionization detector cell filled with 0.15 Torr acetone the xenon pressure and the corresponding VUV laser light generation is optimized. The emerging VUV light is directed through a second lens consisting of LiF ($f = 50$ mm at 248 nm) into the center of the vacuum chamber. The VUV laser light is used for a state-selective resonant excitation of the $B^1\Sigma^+$ state of the CO molecules. The fundamental laser light that is also led through the vacuum chamber finally ionizes the electronically excited molecules [24].

The ionized molecules are collected perpendicular to the surface plane via a detector consisting of a repeller, a flight tube (60-mm length), a microchannel plate (MCP, Galileo 3040) and a phosphor screen. Since the MCPs are sensitive to UV light, the flight tube is necessary to avoid their saturation from stray light of the desorption and detection laser. Additionally, the enhanced signal output of the MCPs is projected onto a phosphor screen to create an image. The signal available at the MCPs as well as the imaged intensity on the screen is proportional to the integral amount of the state-selectively detected molecules.

The detector can image a cone of $\pm 30°$ off the surface normal (diameter of the detector $= 40$ mm). Since the generated VUV-laser light is weak (in the μJ regime) [23] the detection volume is limited to a small region around the center of the chamber within the laser focus. On the other hand, the diameter of the detector is important in the case of a substantial lateral displacement. From two-dimensional imaging experiments performed for different systems [9, 25] the voltages at the repeller and microchannel plates are optimized to minimize deviations related to the flight time within the flight tube and to reduce the amount of molecules escaping the detection volume before entering the flight tube.

If the angular distribution of the desorbing molecules is rather broad due to a substantial part of lateral velocity components along the detection laser beam, portions of the molecules might escape the detection volume. This would be visible as a cut off of the outer parts of the Doppler profiles recorded. Calibration of the detector with a pulsed molecular beam [26] reveals deviations of 4% for maximal velocities of 1800 m s^{-1} observed within our experiments. These deviations could also contribute to the cut off for molecules with large desorption velocity as well as lateral velocity components. However, the signal to noise ratio is not large enough to completely exclude a certain cut off.

Furthermore, the presence of the crystal close to the repeller may lead to field distortions and thus to errors of up to 10%. Such errors are excluded by comparing experimental results that are obtained with and without a bias of 1 kV between the crystal and the repeller. The background signal is subtracted by employing a boxcar integrator running in toggle mode while the detection laser operates at twice the frequency of the desorption laser.

The total signal to noise ratio to be noted within the Doppler profiles is (i) due to intensity variations of successive desorption laser pulses (±15%) and (ii) to intensity variations of the detection laser beam (±3%) within the fundamental, which is worse for the frequency-tripled pulse due to the non-linear nature of creating the VUV pulse. (iii) Further errors within the total intensity may be related to the background-signal subtraction.

2.2 *Details of calculation*

To obtain comparable Doppler profiles and lateral velocity distributions, respectively, from the theoretical approach, quantum dynamical wave packet calculations on ab initio potential energy surfaces (PESs) are performed. The simulations particularly take into account the high dimensionality of the CO/Cr_2O_3(0001) system by considering four degrees of freedom. The laser-induced desorption process is treated within a two-state model: the electronic ground state and the internal CO($5\sigma \rightarrow 2\pi^*$) excitation as the involved electronically excited state. For these states, the challenging generation of four-dimensional ab initio potential energy surfaces is achieved by electronic structure calculations on the configuration interaction (CI) level [19]. The Cr_2O_3(0001) surface is modeled as a Cr_4O_6 cluster that is embedded in a point-charge field. The four considered dimensions are given by the desorption coordinate Z, the polar angles θ and φ of the CO molecule rotation, and one lateral coordinate X. In the experimental studies, cylindrical symmetry about the surface normal is assumed. Then, there is only one lateral coordinate that is independent of the specific direction on the surface. The validity of this approximation is supported

by theoretical investigations to be published elsewhere [27]. Therefore, the lateral coordinate X is assigned to the direction with the strongest potential energy gradients that should cause the most significant part of the lateral dynamics. Following the indication of the ab initio electronic structure calculations, the lateral coordinate X is thus allocated to the short Cr-Cr axis on the Cr-terminated surface (see Fig. 1).

In the quantum dynamical wave packet simulations on these PESs, a stochastic wave packet scheme is employed that includes an incoherent averaging with respect to the residence lifetime of the electronically excited state [28]: for a single quantum trajectory with index n, the laser-induced transition is modeled as a Franck–Condon excitation of the rovibrational ground state to the electronically excited state. After a time evolution in the excited state for a fixed residence lifetime t_n, the wave packet is transferred back to the electronic ground state. During the subsequent time evolution in the electronic ground state, the desorbing wave-packet part is consecutively separated by a grid-change method up to convergence [29]. By calculating $n_{\max} = 70$ quantum trajectories with varying residence lifetime t_n, the distributions of the lateral velocity v_X can be averaged:

$$I(v_X, \tau) = \frac{\sum_{n=1}^{n_{\max}} I(v_X, t_n) \exp(-t_n/\tau)}{\sum_{n=1}^{n_{\max}} \exp(-t_n/\tau)}, \quad (1)$$

assuming an exponential decay of the laser-induced electronic transition [28]. The resonance lifetime τ is determined by requiring the analogously formed desorption probability $P_{\mathrm{des}}(\tau)$ to be in the experimentally estimated range of 1%–10% [14]. For resonance lifetimes of 5–12 fs that are consistent with this desorption probability range, the lifetime-averaged Doppler profiles are very similar, thus showing only a slight dependence on the resonance lifetime. Hence, the resonance lifetime $\tau = 8.8$ fs is used that corresponds to a desorption probability $P_{\mathrm{des}} = 5\%$. The enormous computational effort of calculating 70 quantum trajectories of 1.5-ps duration on a four-dimensional grid with 3.4×10^8 grid points is handled by an efficiently parallelized wave packet code running on massively parallel supercomputers [20]. Finally, the resulting lifetime-averaged lateral velocity distributions can readily be transformed into Doppler profiles. Considering the three different orientations of CO adsorbed on threefold $Cr_2O_3(0001)$, the Doppler profiles are incoherently averaged with regard to the three equivalent adsorption sites (see Fig. 1). To provide an accurate comparison with the experimental results, the Doppler profiles are convoluted with a Gaussian characterized by a full width at half maximum (FWHM) of 0.04 cm^{-1}, which is equal to the experimental detection laser resolution.

3 Results

3.1 *Experimental results*

The Doppler profile of gas-phase CO molecules within the vibrational state $v'' = 0$ and the rotational state $j'' = 7$ at a temperature of 303 K is shown in Fig. 2. The Doppler profile is recorded by varying the fundamental detection wavelength λ in steps of 0.000069 nm around 345 nm and recording 20 desorption pulses per step. The Doppler profile shown is an average of 6–8 measurements. The zero of the spectrum corresponds to the resonant transition frequency at $\tilde{\nu}_0 = 86\,948.80\,\mathrm{cm}^{-1}$ for molecules with no velocity component parallel or antiparallel to the detection laser beam. Velocity components along the detection laser lead to changes within the absorption frequency $\tilde{\nu}$ with respect to the center of absorption $\tilde{\nu}_0$, which is known as the Doppler shift. The Doppler shift is given by

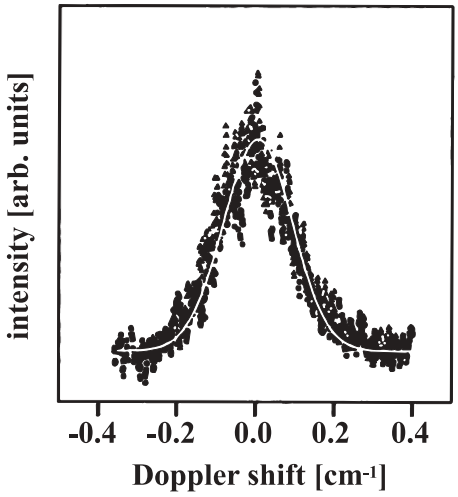

FIGURE 2 Experimental Doppler profile of CO molecules in gas phase within the state $v'' = 0$, $j'' = 7$ at 303 K. The curve indicated by the *solid white line* results from kinetic gas theory (equation (3))

$$\tilde{\nu} - \tilde{\nu}_0 = \tilde{\nu}_0 v/c\,, \quad (2)$$

with v being the velocity component along the detection laser beam and c being the speed of light [30]. The intensity profile of a Doppler-broadened spectral absorption line $I(\tilde{\nu})$ assuming an isotropic three-dimensional velocity distribution is given by

$$I(\tilde{\nu}) = I(\tilde{\nu}_0) \exp\left(-\left[c\frac{(\tilde{\nu} - \tilde{\nu}_0)}{\tilde{\nu}_0 v_{\mathrm{m}}}\right]^2\right), \quad (3)$$

with $I(\tilde{\nu}_0)$ being the intensity within the center of the absorption and v_{m} being the average velocity component parallel or antiparallel to the detection laser beam [30]. Assuming an average thermal velocity of $v_{\mathrm{m}} = \sqrt{2kT/m}$ with k being the Boltzmann constant and $m = 4.6496 \times 10^{-26}$ kg being the mass of a CO molecule, the line fit of Fig. 2 drawn as a white line through the measured spectrum is obtained for the provided gas temperature of $T = 303$ K. For this fit a convolution with the resolution of the detection laser system is not necessary to achieve agreement with the measured spectrum. Further resolution-limiting factors such as pressure broadening or the natural line width can also be neglected. Thus, the experimental resolution is limited by the signal to noise ratio only.

However, desorption can lead to non-isotropic angular and velocity distributions. To consider such anisotropy we adopted a description from photodissociation in the gas phase:

assuming cylindrical symmetry about the surface normal the angular distribution $I(\theta)$ is described via

$$I(\theta) = \frac{1}{4\pi}\left[1 + \beta P_2(\cos\theta)\right], \tag{4}$$

with θ being the angle between surface normal and velocity vector [31]. $P_2(\cos\theta)$ is the second Legendre polynomial. The anisotropy parameter β takes values between +2 (desorption direction purely parallel to the surface normal) and –1 (desorption direction purely perpendicular to the surface normal). For desorption velocity resolved measurements with a detection laser running parallel to the surface we obtain

$$I(\tilde{\nu}) = \frac{1}{2\Delta\tilde{\nu}_D}\left[1 - \tfrac{1}{2}\beta P_2(x_D)\right] \tag{5}$$

by employing the simple approximation of a sharp lateral velocity distribution [31, 32]. Here the total line width $\Delta\tilde{\nu}_D$ also enters the fractional Doppler shift $x_D = (\tilde{\nu} - \tilde{\nu}_0)/\Delta\tilde{\nu}_D$. The anisotropy parameter β is set to +2 as the molecules mainly desorb along the surface normal in our experiments. The line shape of the desorption velocity resolved Doppler profiles finally results in

$$I(\tilde{\nu}) = \frac{1}{2\Delta\tilde{\nu}_D}\left[1 - P_2(x_D)\right]\cos^n\alpha(x_D) \tag{6}$$

by multiplication with the supplementary function $\cos^n\alpha(x_D) = \left(1 + x_D^2\right)^{-n/2}$ that is commonly used in surface science for desorption distributions [5]. This additional factor accounts for the sharper shapes of desorption distributions, thus compensating for the limited flexibility of (4). Ultimately, the employed fit procedure optimizes the two fit parameters $\Delta\tilde{\nu}_D$ and n of the line shape (6).

Figure 3 exhibits desorption velocity resolved Doppler profiles of CO molecules within the state $v'' = 0$, $j'' = 12$ desorbing from a Cr_2O_3(0001) surface after laser excitation. The time delay between desorption and detection is fixed to several values in order to obtain the spectrum as a function of desorption velocity. Doppler profiles for desorption velocities of 145 m s^{-1} (topmost curve), 340 m s^{-1}, 480 m s^{-1},

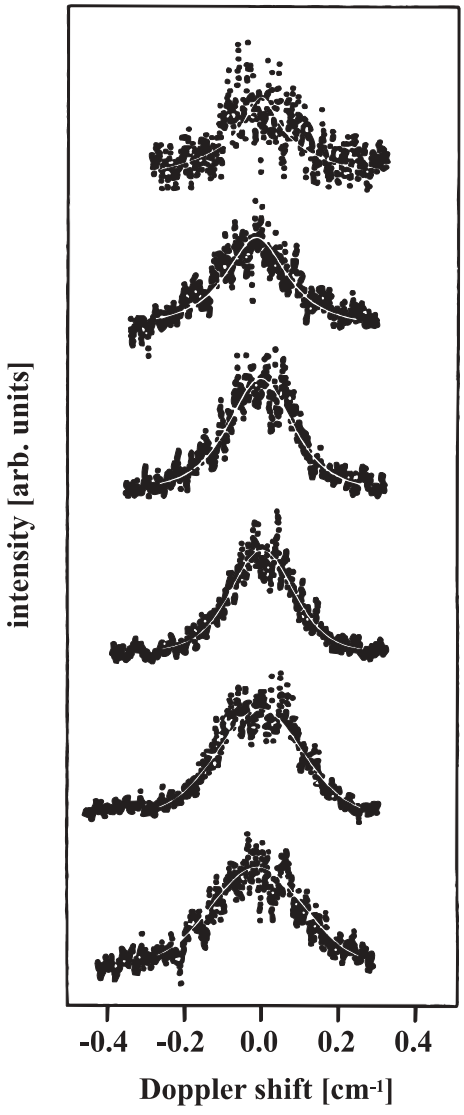

FIGURE 3 Experimental Doppler profiles of CO molecules desorbing from Cr_2O_3(0001) within the state $v'' = 0$, $j'' = 12$ for several desorption velocities: 145 m s^{-1} (*topmost profile*), 340 m s^{-1}, 480 m s^{-1}, 650 m s^{-1}, 1160 m s^{-1} and 1930 m s^{-1} (*lowest profile*). The fitted curves indicated by *solid white lines* result from (6)

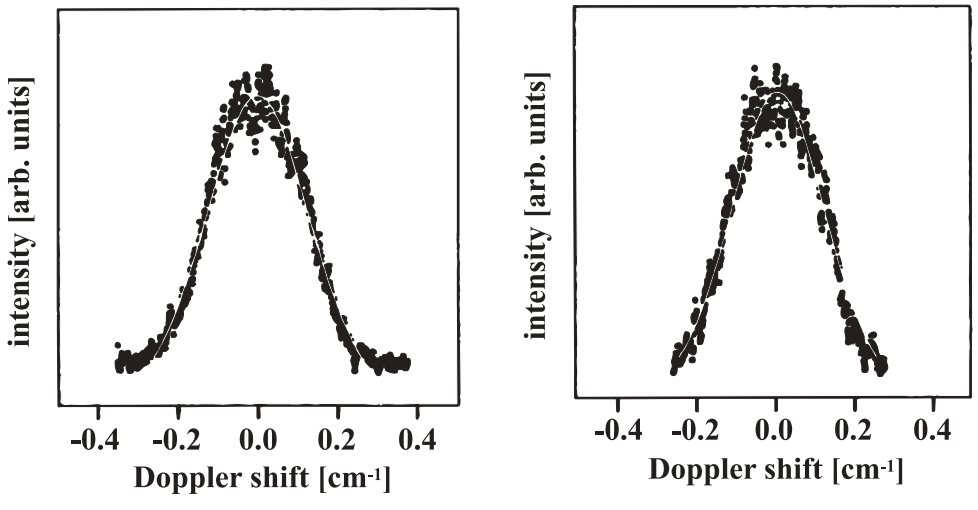

FIGURE 4 Experimental Doppler profiles of CO molecules desorbing from Cr_2O_3(0001) within the states $v'' = 0$, $j'' = 8$ (*left profile*) and $v'' = 0$, $j'' = 31$ (*right profile*) for the desorption velocity 1160 m s^{-1}. The fitted curves indicated by *solid white lines* result from (6)

650 m s^{-1}, 1160 m s^{-1} and 1930 m s^{-1} (lowest curve) are shown. The curves fitted through the spectra result from (6). The maximal Doppler shift is similar for all profiles shown, whereas the shape of the profiles tends to become broader with increasing desorption velocity. For instance, according to the FWHM of the Doppler profiles, lateral velocities of 360 m s^{-1} and 450 m s^{-1} are obtained for slow (340 m s^{-1}) and fast (1160 m s^{-1}) desorption channels, respectively. However, slowly desorbing molecules with a lateral velocity component beyond a limit specified by the detection cone are out of the detection range and thus a cut off within the Doppler profile should be the result. For desorption velocities below 1000 m s^{-1} the detector does not collect all desorbing molecules and such cut off should in principle be observable in the spectra depicted in Fig. 3. But this effect is obscured because of the signal to noise ratio on one hand and the fact that the desorption laser is not a point source on the other hand.

Figure 4 displays desorption velocity resolved Doppler profiles for two different rotational states $v'' = 0$, $j'' = 8$ and $v'' = 0$, $j'' = 31$ in the fast (1160 m s^{-1}) desorption channel. Again, no significant difference of the maximal Doppler shift is found. The lateral velocities resulting from the FWHM of the Doppler profiles amount to 500 m s^{-1} and 480 m s^{-1} for the rotational states $j'' = 8$ and $j'' = 31$, respectively. Hence, no noticeable dependence of the Doppler profiles on the rotational excitation is observed (also compared with respect to the spectra shown in Fig. 3). Concluding the experimental analysis, the lateral motion of the desorbing CO molecules is almost decoupled from normal motion and rotational excitation since the measured Doppler profiles do not significantly depend on the desorption velocity and the rotational state, respectively.

3.2 *Theoretical results*

The experimentally observed Doppler profiles can be directly compared to theoretical results obtained from the stochastic wave packet calculations introduced in Sect. 2.2. By integration over all rotational states and desorption velocities a total lateral velocity distribution is determined. The total Doppler profile results from the lateral velocity distribution by use of (2). The calculated total Doppler profile is depicted in Fig. 5. For comparison both a lateral velocity and a Doppler shift axis are shown.

With regard to the FWHM of the Doppler profile reasonable agreement between experiment and theory is achieved. The FWHM of 0.36 cm^{-1} is equivalent to a lateral velocity of 620 m s^{-1}, which is about 20% larger than the experimental findings. The total width of the Doppler profile of about 0.8 cm^{-1} complies with a maximal lateral velocity of approximately 1380 m s^{-1}. However, this maximal lateral velocity is far out of the detection range in the current experiment. Therefore, the theoretically overestimated lateral velocity is not necessarily in contradiction to the experiment. Future studies taking into account the limited detection cone are expected to give a more consistent comparison [33].

As far as the shape of the Doppler profile is concerned our simulations predict the maximum intensity at a lateral velocity of about 270 m s^{-1}. Thus, a double peak with reduced intensity at the center of the profile is predicted. It is difficult to judge whether this so-called Doppler-split profile [32] is consistent with experimental data. Compared to the experimental results displayed in Fig. 3 such a reduced intensity at the center of the profile cannot be ruled out due to the signal to noise ratio.

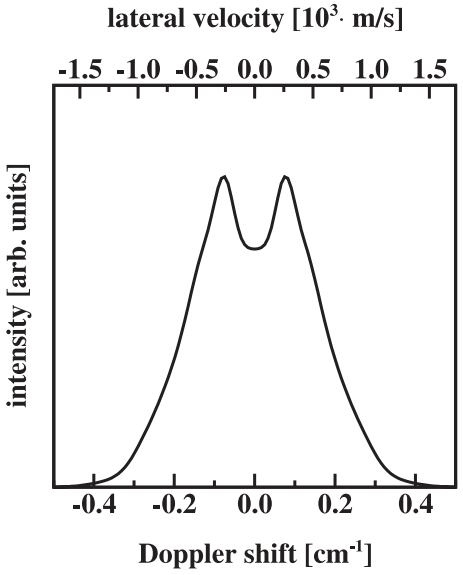

FIGURE 5 Theoretical Doppler profiles and lateral velocity distributions, respectively, of CO molecules desorbing from Cr_2O_3(0001) integrated over all rotational states and desorption velocities

In order to provide a detailed comparison of our theoretical results with experimental data we calculated differential Doppler profiles as well, which are integrated over all desorption velocities but are state resolved with respect to the rotational state. In Fig. 6 the differential Doppler profiles for $j = 12$ and $j = 31$ are illustrated, respectively.

From the FWHM of the Doppler profiles lateral velocities of 590 m s^{-1} and 790 m s^{-1} are calculated for the rotational states $j = 12$ and $j = 31$, respectively. Considering the broad shoulders of the Doppler profile for $j = 31$ to be out of the detection cone the difference between the lateral velocities for the two rotational states should be reduced. The total width of the Doppler profiles is nearly independent of the rotational state, which is consistent with the experimental observation. However, we observe a strong dependence of the shape on the rotational state. While for $j = 12$ a pronounced double-peaked Doppler-split profile is obtained the profile shape for $j = 31$ is characterized by a single-peak structure. Again, a direct comparison of our simulations with experimental data is extremely difficult due to the inferior signal to noise ratio in the experiments. Furthermore, future theoretical studies will clarify whether the assignment of the electronically excited intermediate to an internal CO($5\sigma \rightarrow 2\pi^*$) excitation is justified.

Nevertheless, the dependence of the profile shape on the rotational state of the desorbing molecules is an interesting prediction. Unfortunately, it is very difficult to analyze the origin of this effect in a four-dimensional stochastic wave-packet dynamics. In order to shed light on the underlying mechanism the evolution of a single representative quantum trajectory is followed in time. Preliminary investigations indicate that

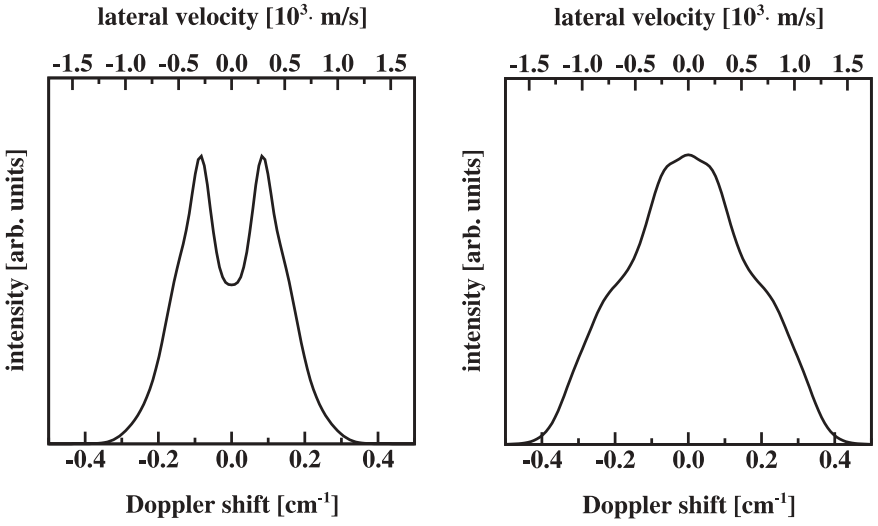

FIGURE 6 Theoretical Doppler profiles and lateral velocity distributions, respectively, of CO molecules desorbing from Cr_2O_3(0001) within the states $j'' = 12$ (*left profile*) and $j'' = 31$ (*right profile*) integrated over all desorption velocities

the origin of the shape dependence of the Doppler profiles on the rotational state can be traced back to dynamical coupling between lateral and rotational motion originating from the topology of the potential energy surfaces involved. For weak rotational excitation the topology of the potential energy surfaces with respect to the lateral coordinate is probed in greater detail compared to strong rotational excitation. While details of this analysis will be published elsewhere [33], this effect is reminiscent of the phenomenon of dynamical steering discussed in recent publications [34].

4 Conclusions

We have demonstrated that lateral velocity distributions can be measured for CO desorbing from an epitaxially grown film of Cr_2O_3(0001)/Cr(110) using Doppler profile analysis of $(1+1')$-REMPI signals of single rovibrational states after inducing desorption with UV-laser light at 6.4 eV. Experimentally, we observe the Doppler profiles and lateral velocity distributions, respectively, to be mainly independent of the desorption velocity. However, as indicated by the analysis presented in Sect. 3.1, the Doppler profiles tend to exhibit a broader shape with increasing desorption velocities.

The appealing feature of the experimental method is its simple realization. The introduction of line width narrowing elements within the laser system (for example an etalon) is relatively easy and far less costly than the utilization of two-dimensional imaging methods. Furthermore, a big advantage of our method is its capability of employing spectroscopic techniques that are prohibitive for two-dimensional imaging because of intensity problems when widening the detection laser beam to a sheet. This fact is of particular importance for desorption processes with rather low cross sections. Here the Doppler profile analysis introduces a much broader applicability.

In addition to these experimental studies, theoretical investigations were performed in order to simulate the experimentally obtained Doppler profiles. For the first time four-dimensional stochastic quantum dynamical wave packet calculations utilizing ab initio potential energy surfaces for the electronic ground state as well as for the electronically excited state involved in the desorption process were performed to simulate a DIET process.

Reasonable quantitative agreement between theory and experiment with respect to the total width and the FWHM of the Doppler profiles was obtained. Furthermore, a dependence of the shape of Doppler profiles on the rotational state is predicted theoretically, suggesting a dynamical steering effect as being the microscopic origin of this phenomenon. As this prediction could not directly be confirmed by the present comparison of experimental and theoretical data, our results underline the need for experimental investigations with an improved signal to noise ratio and further theoretical studies concerning other electronically excited intermediates.

ACKNOWLEDGEMENTS We gratefully acknowledge financial support by the German Science Foundation (DFG, SPP1093) and computer resources provided by the Zentralinstitut für angewandte Mathematik of the Forschungszentrum Jülich and the Rechenzentrum der Max-Planck-Gesellschaft Garching.

REFERENCES

1 X.-L. Zhou, X.-Y. Zhu, J.M. White: Surf. Sci. Rep. **13**, 73 (1991)
2 R.R. Cavanagh, D.S. King, J.C. Stephenson, T.F. Heinz: J. Phys. Chem. **97**, 786 (1993)
3 H.-L. Dai, W. Ho (Eds.): *Laser Spectroscopy and Photochemistry on Metal Surfaces* (World Scientific, Singapore 1995)
4 K. Al-Shamery: Appl. Phys. A: Mater. Sci. Process. **63**, 509 (1996)
5 F.M. Zimmermann, W. Ho: Surf. Sci. Rep. **22**, 127 (1995)
6 W. Ho: J. Phys. Chem. **100**, 13 050 (1996)
7 A.R. Burns: Surf. Sci. **280**, 349 (1993)
8 R. Schwarzwald, A. Mödl, T.J. Chuang: Surf. Sci. **242**, 437 (1991)
9 M. Menges, B. Baumeister, K. Al-Shamery, H.-J. Freund, C. Fischer, P. Andresen: Surf. Sci. **316**, 103 (1994)
10 P.L. Houston: J. Phys. Chem. **91**, 5388 (1987)
11 R.N. Dixon: J. Chem. Phys. **85**, 1866 (1986)
12 H. Guo, P. Saalfrank, T. Seideman: Prog. Surf. Sci. **62**, 239 (1999)
13 T. Klüner, H.-J. Freund, V. Staemmler, R. Kosloff: Phys. Rev. Lett. **80**, 5208 (1998)
14 S. Thiel, M. Pykavy, T. Klüner, H.-J. Freund, R. Kosloff, V. Staemmler: Phys. Rev. Lett. **87**, 077 601 (2001); S. Thiel, M. Pykavy, T. Klüner, H.-J. Freund, R. Kosloff, V. Staemmler: J. Chem. Phys. **116**, 762 (2002)
15 D. Menzel, R. Gomer: J. Chem. Phys. **41**, 3311 (1964); P.A. Redhead: Can. J. Phys. **42**, 886 (1964)

16 P.R. Antoniewicz: Phys. Rev. B **21**, 3811 (1980)
17 H. Guo: J. Chem. Phys. **106**, 1967 (1997); P. Saalfrank, G. Boendgen, K. Finger, L. Pesce: Chem. Phys. **251**, 51 (2000); F.M. Zimmermann: Surf. Sci. **390**, 174 (1997); L. Pesce, T. Gerdts, U. Manthe, P. Saalfrank: Chem. Phys. Lett. **288**, 383 (1998); N. Balasubramanian, N. Sathyarmurthy, J.W. Gadzuk: Chem. Phys. Lett. **242**, 490 (1995)
18 A.R. Burns, E.B. Stechel, D.R. Jennison, Y.S. Li: J. Chem. Phys. **101**, 6318 (1994); H. Guo, T. Seideman: J. Chem. Phys. **103**, 9062 (1995); P. Saalfrank: Surf. Sci. **390**, 1 (1997); T. Hertel, M. Wolf, G. Ertl: J. Chem. Phys. **102**, 3414 (1995)
19 M. Pykavy, V. Staemmler, O. Seiferth, H.-J. Freund: Surf. Sci. **479**, 11 (2001); M. Pykavy, S. Thiel, T. Klüner: J. Phys. Chem. B **106**, 12 556 (2002)
20 S. Borowski, S. Thiel, T. Klüner, H.-J. Freund, R. Tisma, H. Lederer: Comput. Phys. Commun. **143**, 162 (2002)
21 C. Xu, M. Haßel, H. Kuhlenbeck, H.-J. Freund: Surf. Sci. **258**, 23 (1991)
22 C. Xu, B. Dillmann, H. Kuhlenbeck, H.-J. Freund: Phys. Rev. Lett. **67**, 3551 (1991)
23 H. Rottke, H. Zacharias: Opt. Commun. **55**, 87 (1985)
24 K. Al-Shamery, I. Beauport, H.-J. Freund, H. Zacharias: Chem. Phys. Lett. **222**, 107 (1994); I. Beauport: PhD thesis, Bochum, Germany (1996)
25 M. Wilde, K. Fukutani, Y. Murata, M. Kampling, K. Al-Shamery, H.-J. Freund: Surf. Sci. **427**–**428**, 27 (1999)
26 C. Fischer: PhD thesis, Göttingen, Germany (1994)
27 S. Borowski, T. Klüner, H.-J. Freund: J. Chem. Phys., accepted
28 J.W. Gadzuk, L.R. Richter, S.A. Buntin, D.S. King, R.R. Cavanagh: Surf. Sci. **235**, 317 (1990); J.W. Gadzuk: Surf. Sci. **342**, 345 (1995)
29 R. Heather, H. Metiu: J. Chem. Phys. **86**, 5009 (1987)
30 W. Demtröder: *Laserspektroskopie* (Springer, Heidelberg 1993)
31 R. Schmiedl, H. Dugan, W. Meier, K.H. Welge: Z. Phys. A **304**, 137 (1982)
32 R. Vasudev, R.N. Zare, R.N. Dixon: J. Chem. Phys. **80**, 4863 (1984)
33 S. Borowski, T. Klüner, H.-J. Freund: in preparation
34 A. Groß, S. Wilke, M. Scheffler: Phys. Rev. Lett. **75**, 2718 (1995); A. Groß, M. Scheffler: Prog. Surf. Sci. **53**, 187 (1996)